ENCLOSURE 6

TENNESSEE VALLEY AUTHORITY
BROWNS FERRY NUCLEAR PLANT (BFN)
UNIT 1

TECHNICAL SPECIFICATIONS (TS) CHANGE TS-431
EXTENDED POWER UPRATE (EPU)

CDI REPORT NO. 09-24NP, "STRESS ASSESSMENT OF BROWNS FERRY NUCLEAR UNIT 1 STEAM DRYER TO 110% OLTP POWER LEVEL," REVISION 0

(NON-PROPRIETARY VERSION)

Attached is the non-proprietary version of CDI Report No. 09-24NP, "Stress Assessment of Browns Ferry Nuclear Unit 1 Steam Dryer to 110% OLTP Power Level."

This Document Does Not Contain Continuum Dynamics, Inc. Proprietary Information

CDI Report No. 09-24NP

Stress Assessment of Browns Ferry Nuclear Unit 1 Steam Dryer to 110% OLTP Power Level

Revision 0

Prepared by

Continuum Dynamics, Inc.
34 Lexington Avenue
Ewing, NJ 08618

Prepared under Purchase Order No. 00053157 for

TVA / Browns Ferry Nuclear Plant
Nuclear Plant Road, P. O. Box 2000 PAB-2M
Decatur, AL 35609

Approved by

Alan J. Bilanin

Reviewed by

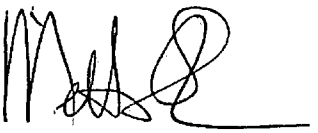

Milton E. Teske

August 2009

This report complies with Continuum Dynamics, Inc. Nuclear Quality Assurance Program currently in effect.

Executive Summary

The finite element model and analysis methodology, used to assess stresses induced by the flow of steam through the steam dryer at Brown Ferry Nuclear Unit 1 (BFN1), are described and applied to obtain stresses at 110% Originally Licensed Thermal Power (OLTP) conditions. The resulting stresses are assessed for compliance with the ASME B&PV Code, Section III, subsection NG, for the load combination corresponding to normal operation (the Level A Service Condition). The results presented pertain to the current (as of report date) configuration of the BFN1 steam dryer including modifications that have been incorporated to improve stress margins for 110% OLTP and ultimately also EPU operation. In particular, changes to the tie-bars and steam dam gussets have been incorporated to promote alternating stress ratios above 2.0 at 110% OLTP conditions.

The analysis is carried out in the frequency domain, which confers a number of useful computational advantages over a time-accurate transient analysis including the ability to assess the effects of frequency scalings in the loads without the need for additional finite element calculations. [[

[3]]] The analysis develops a series of unit stress solutions corresponding to the application of a unit pressure at a MSL at specified frequency, f. Each unit solution is obtained by first calculating the associated acoustic pressure field using a separate analysis that solves the damped Helmholtz equation within the steam dryer [1]. This pressure field is then applied to a finite element structural model of the steam dryer and the harmonic stress response at frequency, f, is calculated using the commercial ANSYS 10.0 finite element analysis software. This stress response constitutes the unit solution and is stored as a file for subsequent processing. Once all unit solutions have been computed, the stress response for any combination of MSL pressure spectrums (obtained by Fast Fourier Transform of the pressure histories in the MSLs) is determined by a simple matrix multiplication of these spectrums with the unit solutions.

Results obtained from application of the methodology to the BFN1 steam dryer show that at nominal 110% OLTP operation (no frequency shifts) the minimum alternating stress ratio (SR-a) anywhere on the steam dryer, excluding secondary structural members, is SR-a=2.01. The loads used to obtain this value account for all the end-to-end biases and uncertainties in the loads model [2] and finite element analysis. It is noted that:

(i) The signals account for the revised biases and uncertainties in the 60-70 Hz and 70-100 Hz frequency ranges. For various reasons the ACM was not recalibrated over the new frequency ranges (such a recalibration is resource-intensive and would lead to a new revision of the ACM). As a result, the biases and uncertainties in the new intervals are more conservative and higher than they would otherwise be, had such a recalibration of the ACM been performed.

(ii) It is known that the signals used to estimate acoustic loads contain significant non-acoustic contributions referred to collectively as plant noise (e.g., pipe vibrations). However, to expedite qualification, no noise removal has been performed for the analyses contained herein.

Both of these load details increase conservatism in the analysis. Moreover, to account for uncertainties in the modal frequency predictions of the finite element model, the stresses are also computed for loads that are shifted in the frequency domain by ±2.5%, ±5%, ±7.5% and ±10%. The minimum alternating stress ratio encountered at any frequency shift is found to be SR-a=2.01 occurring at the +10% shift. The stress ratio due to maximum stresses (SR-P) is SR-P=1.42 without frequency shifts and SR-P=1.36 when frequency shifts are considered.

These results exclude stresses associated with secondary structural members. When all structural parts are considered, including secondary structural members that are not needed for maintaining structural integrity, additional high stress locations emerge. All of these locations involve the T-bar originally required for transportation and assembly of the dryer. A separate analysis has been conducted to determine the stress condition and position retention capability of the structure if the highest stressed nodes are removed from the model to simulate a conservatively postulated, localized failed condition. This analysis shows that limiting alternating stress ratio on the T-bar welds becomes SR-a=2.17 at 110% OLTP.

Given that the alternating stress ratio SR-a obtained using any of two 110% OLTP predictive stress methods remains above 2.01 at all frequency shifts together with the comparatively small dependence of SR-P upon acoustic loads, the current Unit 1 dryer qualifies for operation at 110% OLTP conditions with regard to stress evaluation.

Table of Contents

1. Introduction and Purpose

Plans to qualify the Browns Ferry nuclear plant for operation at 110% Original Licensed Thermal Power (OLTP) operating condition require an assessment of the steam dryer stresses experienced under the increased loads. The steam dryer loads due to pressure fluctuations in the main steam lines (MSLs) are potentially damaging and the cyclic stresses from these loads can produce fatigue cracking if loads are sufficiently high. The industry has addressed this problem with physical modifications to the dryers, as well as a program to define steam dryer loads and their resulting stresses. The purpose of the stress analysis discussed here is to calculate the maximum and alternating stresses generated during 110% OLTP and determine the margins that exist when compared to stresses that comply with the ASME Code (ASME B&PV Code, Section III, subsection NG).

The stress analysis considered here pertains to the Browns Ferry Unit 1 (BFN1) steam dryer in its current configuration at the time of submission of this report. As such, it incorporates recent design changes introduced to improve stress ratios at 110% OLTP and ultimately also extended power uprate (EPU) operation. These changes include redesigned tie bars to alleviate stresses at the tie bar ends and the addition of gussets to help support the steam dam.

The stress analysis of the modified BFN1 steam dryer establishes whether the existing and planned modifications are adequate for sustaining structural integrity and preventing future weld cracking under planned 110% OLTP and EPU operating conditions. The load combination considered here corresponds to normal operation (the Level A Service Condition) and includes fluctuating pressure loads developed from BFN1 main steam line data, and weight. Level B service conditions, which include seismic loads, are not included in this evaluation. The fluctuating pressure loads, induced by the flowing steam, are predicted by processing main steam line (MSL) pipe strain gage measurements using a separate acoustic circuit analysis of the steam dome and main steam lines [3]. It is known that the MSL strain gage measurements also contain non-acoustic contributions, collectively referred to as 'plant noise' (e.g., pipe vibrations, operating machinery and measurement noise) which physically do not contribute to dryer acoustic loads. In previous analyses [4] it was attempted to subtract this non-acoustic noise using low power measurements. To expedite qualification of the dryer however, no low power noise subtraction has been performed in the present analysis.

[[

[3]]] This approach also affords a number of additional computational advantages over transient simulations including: [[[3]]]

[[

(3)]] This last advantage is realized through the use of "unit" solutions representing the stress distribution resulting from the application of a unit fluctuating pressure at one of the MSLs at a particular frequency. [[
(3)]]

This report describes the overall methodology used to obtain the unit solutions in the frequency domain and how to assemble them into a stress response for a given combination of pressure signals in the MSLs. This is followed by details of the BFN1 steam dryer finite element model including the elements used and overall resolution, treatment of connections between elements, the hydrodynamic model, the implementation of structural damping and key idealizations/assumptions inherent to the model. Post-processing procedures are also reviewed including the computation of maximum and alternating stress intensities, identification of high stress locations, adjustments to stress intensities at welds, and evaluation of stress ratios used to establish compliance with the ASME Code. The results in terms of stress intensity distributions and stress ratios are presented next, together with PSDs of the dominant stress components.

2. Methodology

2.1 Overview

Based on previous analysis undertaken at Quad Cities Units 1 and 2, the steam dryer can experience strong acoustic loads due to the fluctuating pressures in the MSLs connected to the steam dome containing the dryer. C.D.I. has developed an acoustic circuit model (ACM) that, given a collection of strain gage measurements [5] of the fluctuating pressures in the MSLs, predicts the acoustic pressure field anywhere inside the steam dome and on the steam dryer [1-3]. The ACM is formulated in frequency space and contains two major components that are directly relevant to the ensuing stress analysis of concern here. [[

[3]]]

[[

[3]]]

[[

[3]]

2.2 [[[3]]
[[

[3]]

[[

[3]]]

2.3 Computational Considerations

Focusing on the structural computational aspects of the overall approach, there are a number of numerical and computational considerations requiring attention. The first concerns the transfer of the acoustic forces onto the structure, particularly the spatial and frequency resolutions. The ANSYS finite element program inputs general distributed pressure differences using a table format. This consists of regular 3D rectangular (i.e., block) $n_x \times n_y \times n_z$ mesh where n_α is the number of mesh points in the i-th Cartesian direction and the pressure difference is provided at each mesh point (see Section 3.10). These tables are generated separately using a program that reads the loads provided from the ACM software, distributes these loads onto the finite element mesh using a combination of interpolation procedures on the surface and simple diffusion schemes off the surface (off-surface loads are required by ANSYS to ensure proper interpolation of forces), and written to ASCII files for input to ANSYS. A separate load file is written at each frequency for the real and imaginary component of the complex force.

The acoustic field is stored at 5 Hz intervals from 0 to 250 Hz. While a 5 Hz resolution is sufficient to capture frequency dependence of the acoustic field (i.e., the pressure at a point varies gradually with frequency), it is too coarse for representing the structural response especially at low frequencies. For 1% critical structural damping, one can show that the frequency spacing needed to resolve a damped resonant peak at natural frequency, f_n, to within 5% accuracy is $\Delta f = 0.0064 \times f_n$. Thus for f_n=10 Hz where the lowest structural response modes occur, a frequency interval of 0.064 Hz or less is required. In our calculations we require that 5% maximum error be maintained over the range from f_n=5 Hz to 250 Hz resulting in a finest frequency interval of 0.0321 Hz at the low frequency end (this adequately resolves all structural modes up to 250 Hz). Since there are no structural modes between 0 to 5 Hz, a 0.5 Hz spacing is used over this range with minimal (less than 5%) error. The unit load, $\hat{\mathbf{f}}_n(\omega, \mathbf{R})$, at any frequency, ω_k, is obtained by linear interpolation of the acoustic solutions at the two nearest frequencies, ω_i and ω_{i+1}, spaced 5 Hz apart. Linear interpolation is sufficient since the pressure load varies slowly over the 5 Hz range (linear interpolation of the structural response would not be acceptable over this range since it varies much more rapidly over the same interval).

Solution Management

[[

[3]]]

[[

[3]]]

Structural Damping

In harmonic analysis one has a broader selection of damping models than in transient simulations. A damping factor, z, of 1% critical damping is used in the structural analysis. In transient simulations, this damping can only be enforced exactly at two frequencies (where the damping model is "pinned"). Between these two frequencies the damping factor can by considerably smaller, for example 0.5% or less depending on the pinning frequencies. Outside the pinning frequencies, damping is higher. With harmonic analysis it is straightforward to enforce very close to 1% damping over the entire frequency range. In this damping model, the damping matrix, **D**, is set to

$$\mathbf{D} = \frac{2z}{\omega}\mathbf{K} \tag{7}$$

where **K** is the stiffness matrix and ω the forcing frequency. One can show that with this model the damping factor varies between 0.995% and 1.005% which is a much smaller variation than using the pinned model required in transient simulation.

Load Frequency Rescaling

One way to evaluate the sensitivity of the stress results to approximations in the structural modeling and applied loads is to rescale the frequency content of the applied loads. In this procedure the nominal frequencies, ω_k, are shifted to $(1+\lambda)\omega_k$, where the frequency shift, λ, ranges between $\pm 10\%$, and the response recomputed for the shifted loads. The objective of the frequency shifting can be explained by way of example. Suppose that in the actual dryer a strong structural-acoustic coupling exists at a particular frequency, ω^*. This means that the following conditions hold simultaneously: (i) the acoustic signal contains a significant signal at ω^*; (ii) the structural model contains a resonant mode of natural frequency, ω_n, that is near ω^*; and (iii) the associated structural mode shape is strongly coupled to the acoustic load (i.e., integrating the product of the mode shape and the surface pressure over the steam dryer surface produces a significant modal force). Suppose now that because of discretization errors and modeling idealizations that the predicted resonance frequency differs from ω^* by a small amount (e.g., 1.5%). Then condition (ii) will be violated and the response amplitude therefore significantly

diminished. By shifting the load frequencies one re-establishes condition (ii) when $(1+\lambda)\omega^*$ is near ω_n. The other two requirements also hold and a strong structural acoustic interaction is restored.

[[

[3]]]

Evaluation of Maximum and Alternating Stress Intensities

Once the unit solutions have been obtained, the most intensive computational steps in the generation of stress intensities are: (i) the FFTs to evaluate stress time histories from (5); and (ii) the calculation of alternating stress intensities. [[

[3]]]

The high computational penalty incurred in calculating the alternating stress intensities is due to the fact that this calculation involves comparing the stress tensors at every pair of points in the stress history. This comparison is necessary since in general the principal stress directions can vary during the response, thus for N samples in the stress history, there will be (N-1)N/2 such pairs or, for N=64K (the number required to accurately resolve the spectrum up to 250 Hz in 0.01 Hz intervals), 2.1×10^9 calculations per node each requiring the determination of the roots to a cubic polynomial. [[

[3]]]

3. Finite Element Model Description

A description of the ANSYS model of the Browns Ferry Unit 1 steam dryer follows.

3.1 Steam Dryer Geometry

A geometric representation of the Browns Ferry steam dryer was developed from available drawings (provided by TVA and included in the design record file, DRF-TVA-250B) within the Workbench module of ANSYS. The completed model is shown in Figure 1. This model includes the following modifications made to the Browns Ferry Unit 1 steam dryer on-site and additional modifications for 110% OLTP and EPU operation. These are as follows:

On-Site Modifications

(i) The 0.5 inch thick old outer hoods were cut away and replaced with 1 inch thick outer hoods.
(ii) Channel-shaped hood assemblies composed of 1 inch thick plates were added to the outer hoods.
(iii) The vertical hood supports located underneath the hood were cut away following the replacement with the thicker outer hood and exterior hood reinforcement assemblies.
(iv) The top tie rods were replaced with thicker new ones. The gussets on the top of the outer hoods supporting the steam dam plate were cut away to facilitate installation of the new tie bars and possibly alleviate local stresses.
(v) The cover plates were replaced by new ones that are 1 in thick.
(vi) The outermost sections (the parts between the upper support ring and outer vane bank) of the supporting beam spanning the dryer were removed.

Previous analysis [8] showed significant stresses at the welds where the thicker tie bars (item (iv)) connect to the top cover plates which would result in alternating stress ratios at EPU below the target level of 2.0. Therefore, additional design modifications have been made to reduce these stresses to target levels. These changes are as follows:

Additional Modifications Added to Prepare for EPU Operation

(vii) Remove the thicker tie bars connecting to the inner hoods (i.e., those connecting the inner to inner hoods and those connecting the inner to middle hoods) and replace them with ones having tapered and flared ends to more evenly distribute loads at the end connections.
(viii) Similarly, replace the thicker tie bars connecting to the outer hoods with the modified ones having flared and tapered ends. However, rather than completely removing the existing tie bars, part of it is retained to support the lock gusset and restrain motion of the steam dam. The portion extending between the steam dam to the middle hood is removed.
(ix) Add three additional gussets to support each of the two steam dams.

At the time of submission of this report, the actual dryer configuration contains all of the modifications above. They have also been incorporated into the BFN1 steam dryer model used to generate the results presented in this report. The modified areas are shown in Figure 2 and Figure 3.

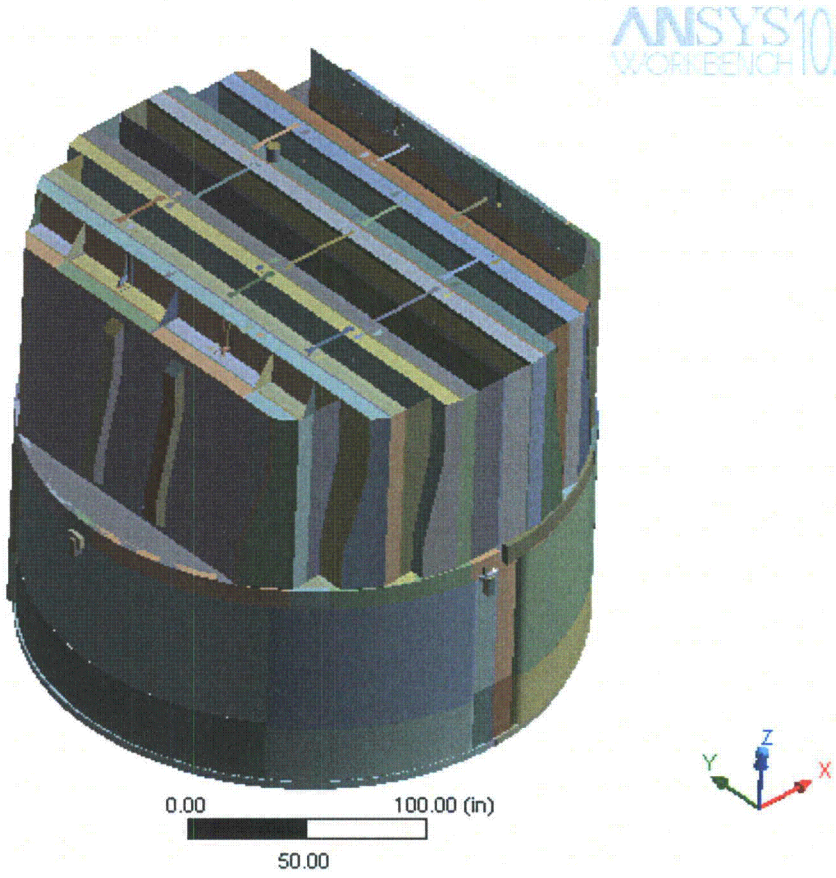

Figure 1. Overall geometry of the Browns Ferry Unit 1 steam dryer model.

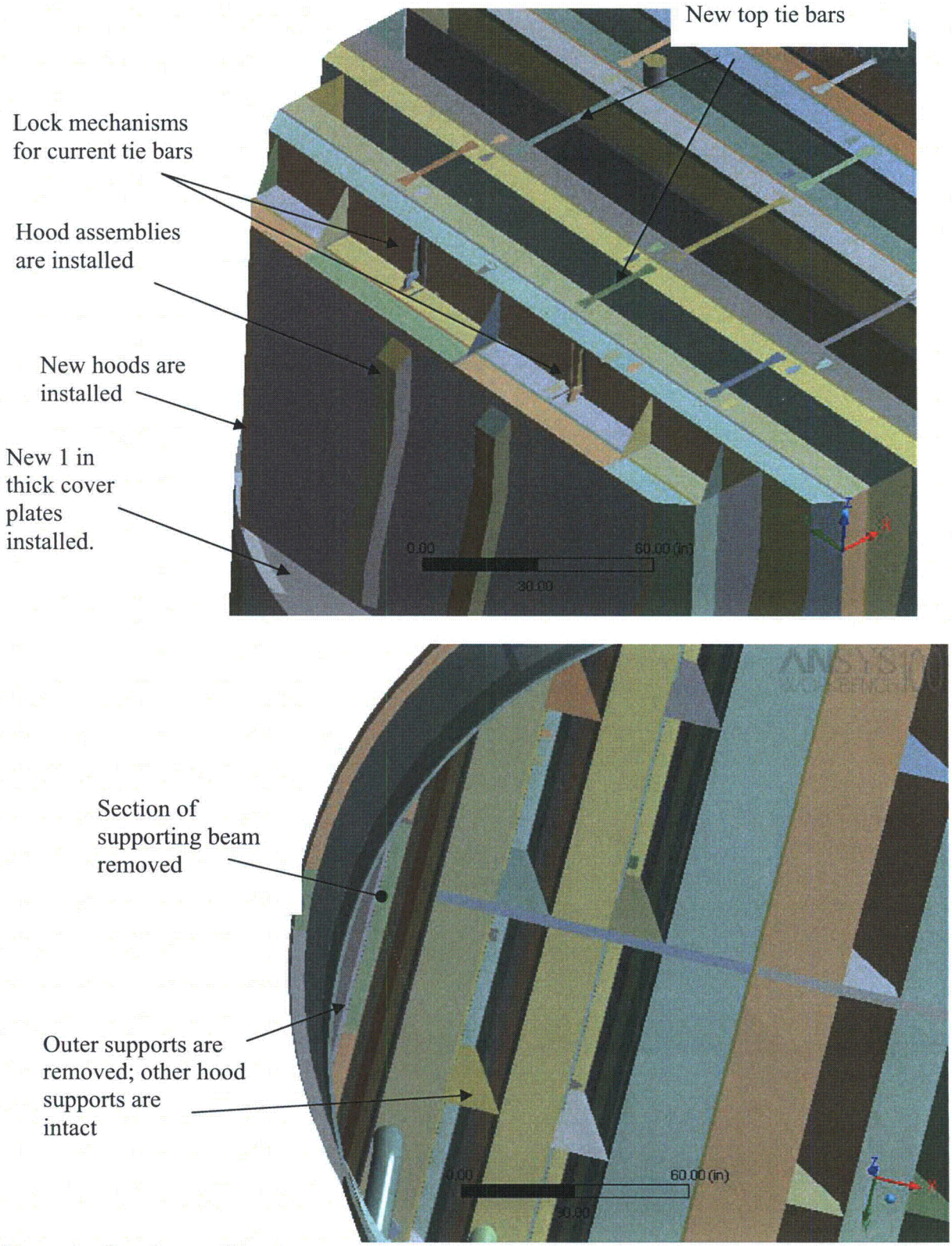

Figure 2. On-site modifications accounted for in the model and associated geometrical details.

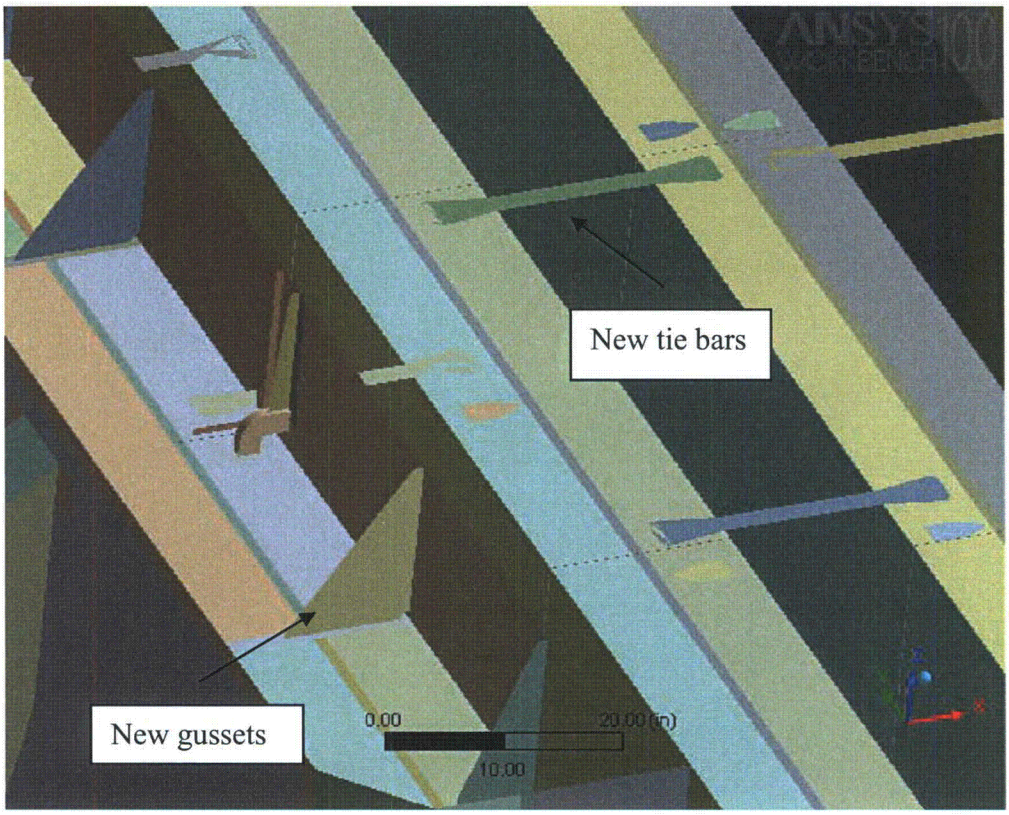

Figure 3. BFN1 modifications involving tie bars and additional steam dam gussets to improve stress margins.

3.2 Material Properties

The steam dryer is constructed from Type 304 stainless steel and has an operating temperature of 550°F. Properties used in the analysis are summarized below in Table 1.

Table 1. Material properties.

	Young's Modulus (10^6 psi)	Density (lbm/in^3)	Poisson's Ratio
structural steel	25.55	0.284	0.3
structural steel with added water inertia	25.55	1.055	0.3

The structural steel modulus is taken from Appendix A of the ASME Code for Type 304 Stainless Steel at an operating temperature 550°F. The effective properties of perforated plates and submerged parts are discussed in Sections 3.4 and 3.6. Note that the increased effective density for submerged components is only used in the harmonic analysis. When calculating the stress distribution due to the static dead weight load, the unmodified density of steel (0.284 lbm/in^3) is used throughout.

3.3 Model Simplifications

The following simplifications were made to achieve reasonable model size while maintaining good modeling fidelity for key structural properties:

- Perforated plates were approximated as continuous plates using modified elastic properties designed to match the static and modal behaviors of the perforated plates. The perforated plate structural modeling is summarized in Section 3.4 and Appendix C of [8].

- The drying vanes were replaced by point masses attached to the corresponding trough bottom plates and vane bank top covers. The bounding perforated plates, vane bank end plates, and vane bank top covers were explicitly modeled (see Section 3.5).

- The added mass properties of the lower part of the skirt below the reactor water level were obtained using a separate hydrodynamic analysis (see Section 3.6).

- [[

  (3)]]

- Four steam dryer support brackets that are located on the reactor vessel and spaced at 90° intervals were explicitly modeled (see Section 3.9).

- Most welds were replaced by node-to-node connections; interconnected parts share common nodes along the welds. In other locations the constraint equations between nodal degrees of freedom were introduced as described in Section 3.9.

3.4 Perforated Plate Model

The perforated plates were modeled as solid plates with adjusted elastic and dynamic properties. Properties of the perforated plates were assigned according to the type and size of perforation. Based on [10], for an equilateral square pattern with given hole size and spacing, the effective moduli of elasticity were found.

The adjusted properties for the perforated plates are shown in Table 2 as ratios to material properties of structural steel, provided in Table 1. Locations of perforated plates are classified by steam entry / exit vane bank side and vertical position.

Tests were carried out to verify that this representation of perforated plates by continuous ones with modified elastic properties preserves the modal properties of the structure. These tests are summarized in Appendix C of [8] and compare the predicted first modal frequency for a cantilevered perforated plate against an experimentally measured value. The prediction was obtained for a 40% open area plate (the maximum open area ratio of the perforated plates at BFN1, as seen in Table 2) using the analytical formula for a cantilevered plate and the modified Young's modulus and Poisson's ratio given by O'Donnell [10]. The measured and predicted frequencies are in close agreement, differing by less than 3%.

[[

[3]]]

[[

(3)]]

Figure 4. [[(3)]]

Table 2. Material properties of perforated plates.

[[

(3)]]

3.5 Vane Bank Model

The vane bank assemblies consist of many vertical angled plates that are computationally expensive to model explicitly, since a prohibitive number of elements would be required. These parts have significant weight which is transmitted through the surrounding structure, so it is important to capture their gross inertial properties. Here the vane banks are modeled as a collection of point masses located at the center of mass for each vane bank section (Figure 4). The following masses were used for the vane bank sections, based on data found on provided drawings:

inner banks, 1575 lbm, 4 sections per bank;

middle banks, 1450 lbm, total 4 sections per bank; and
outer banks, 1515 lbm, 3 sections per bank.

These masses were applied to the base plates and vane top covers using the standard ANSYS point mass modeling option, element MASS21. ANSYS automatically distributes the point mass inertial loads to the nodes of the selected structure. The distribution algorithm minimizes the sum of the squares of the nodal inertial forces, while ensuring that the net forces and moments are conserved. Vane banks are not exposed to main steam lines directly, but rather shielded by the hoods.

The collective stiffness of the vane banks is expected to be small compared to the surrounding support structure and is neglected in the model. In the static case it is reasonable to expect that this constitutes a conservative approach, since neglecting the stiffness of the vane banks implies that the entire weight is transmitted through the adjacent vane bank walls and supports. In the dynamic case the vane banks exhibit only a weak response since (i) they have large inertia so that the characteristic acoustically-induced forces divided by the vane masses and inertias yield small amplitude motions, velocities and accelerations; and (ii) they are shielded from acoustic loads by the hoods, which transfer dynamic loads to the rest of the structure. Thus, compared to the hoods, less motion is anticipated on the vane banks so that approximating their inertial properties with equivalent point masses is justified. Nevertheless, the bounding parts, such as perforated plates, side panels, and top covers, are retained in the model. Errors associated with the point mass representation of the vane banks are compensated for by frequency shifting of the applied loads.

3.6 Water Inertia Effect on Submerged Panels

Water inertia was modeled by an increase in density of the submerged structure to account for the added hydrodynamic mass. This added mass was found by a separate hydrodynamic analysis (included in DRF-TVA-250B supporting this report) to be 0.1928 lbm/in^2 on the submerged skirt area. This is modeled by effectively increasing the material density for the submerged portions of the skirt. Since the skirt is 0.25 inches thick, the added mass is equivalent to a density increase of 0.771 lbm/in^3. This added water mass was included in the ANSYS model by appropriately modifying the density of the submerged structural elements when computing harmonic response. For the static stresses, the unmodified density of steel is used throughout.

3.7 Structural Damping

Structural damping was defined as 1% of critical damping for all frequencies. This damping is consistent with guidance given on pg. 10 of NRC RG-1.20 [14].

3.8 Mesh Details and Element Types

Shell elements were employed to model the skirt, hoods, perforated plates, side and end plates, trough bottom plates, reinforcements, base plates and cover plates. Specifically, the four-node, Shell Element SHELL63, was selected to model these structural components. This element models bending and membrane stresses, but omits transverse shear. The use of shell elements is appropriate for most of the structure where the characteristic thickness is small compared to the other plate dimensions. For thicker structures, such as the upper and lower

support rings, solid brick elements were used to provide the full 3D stress. Tie bars at dryer vane bank mid-height were modeled with BEAM188 beam elements. The elements SURF154 are used to assure proper application of pressure loading to the structure. Mesh details and element types are shown in Table 3 and Table 4, respectively.

The mesh is generated automatically by ANSYS with refinement near edges. The maximum allowable mesh spacing is specified by the user. Here a 2.5 inch maximum allowable spacing is specified everywhere except in the following areas: drain pipes (2 inch maximum spacing); perforated plates (2 inches); and the curved portions of the drain channels (1.5 inches). Details of the finite element mesh are shown in Figure 6. Numerical experiments carried out using the ANSYS code applied to simple analytically tractable plate structures with dimensions and mesh spacings similar to the ones used for the steam dryer, confirm that the natural frequencies are accurately recovered (less than 1% errors for the first modes). These errors are compensated for by the use of frequency shifting.

3.9 Connections Between Structural Components

Most connections between parts are modeled as node-to-node connections. This is the correct manner (i.e., within the finite element framework) of joining elements away from discontinuities. At joints between shells, this approach omits the additional stiffness provided by the extra weld material. Also, locally 3D effects are more pronounced. The latter effect is accounted for using weld factors. The deviation in stiffness due to weld material is negligible, since weld dimensions are on the order of the shell thickness. The consequences upon modal frequencies and amplitude are, to first order, proportional to t/L where t is the thickness and L a characteristic shell length. The errors committed by ignoring additional weld stiffness are thus small and readily compensated for by performing frequency shifts.

When joining shell and solid elements, however, the problem arises of properly constraining the rotations, since shell element nodes contain both displacement and rotational degrees of freedom at every node whereas solid elements model only the translations. A node-to-node connection would effectively appear to the shell element as a simply supported, rather than (the correct) cantilevered restraint and significantly alter the dynamic response of the shell structure.

To address this problem, constraint equations are used to properly connect adjacent shell- and solid-element modeled structures. Basically, all such constraints express the deflection (and rotation for shell elements) of a node, $\mathbf{R}_1$, on one structural component in terms of the deflections/rotations of the corresponding point, $\mathbf{P}_2$, on the other connected component. Specifically, the element containing $\mathbf{P}_2$ is identified and the deformations at $\mathbf{P}_2$ determined by interpolation between the element nodes. The following types of shell-solid element connections are used in the steam dryer model including the following:

1. Connections of shell faces to solid faces (Figure 7a). While only displacement degrees of freedom are explicitly constrained, this approach also implicitly constrains the rotational degrees of freedom when multiple shell nodes on a sufficiently dense grid are connected to the same solid face.
2. Connections of shell edges to solids (e.g., connection of the bottom of closure plates with the upper ring). Since solid elements do not have rotational degrees of freedom, the

coupling approach consisted of having the shell penetrate into the solid by one shell thickness and then constraining both the embedded shell element nodes (inside the solid) and the ones located on the surface of the solid structure (see Figure 7b). Numerical tests involving simple structures showed that this approach and penetration depth reproduce both the deflections and stresses of the same structure modeled using only solid elements or ANSYS' bonded contact technology. Continuity of rotations and displacements is achieved.

The use of constraint conditions rather than the bonded contacts advocated by ANSYS for connecting independently meshed structural components confers better accuracy and useful numerical advantages to the structural analysis of the steam dryer including better conditioned and smaller matrices. The smaller size results from the fact that equations and degrees of freedom are eliminated rather than augmented (in Lagrange multiplier-based methods) by additional degrees of freedom. Also, the implementation of contact elements relies on the use of very high stiffness elements (in penalty function-based implementations) or results in indefinite matrices (Lagrange multiplier implementations) with poorer convergence behavior compared to positive definite matrices.

The upper support ring rests on four support blocks which resist vertical and lateral displacement. Because the contact region between the blocks and upper support ring is small, the ring is considered free to rotate about the radial axis. Specifically nodal constraints (zero relative displacement) are imposed over the contact area between the steam dryer upper support ring and the support blocks. Two nodes on each support block are fixed as indicated in Figure 8. One node is at the center of the support block surface facing the vessel and the other node is 0.5" offset inside the block towards the steam dryer, half way to the nearest upper support ring node. This arrangement approximates the nonlinear contact condition where the ring can tip about the block.

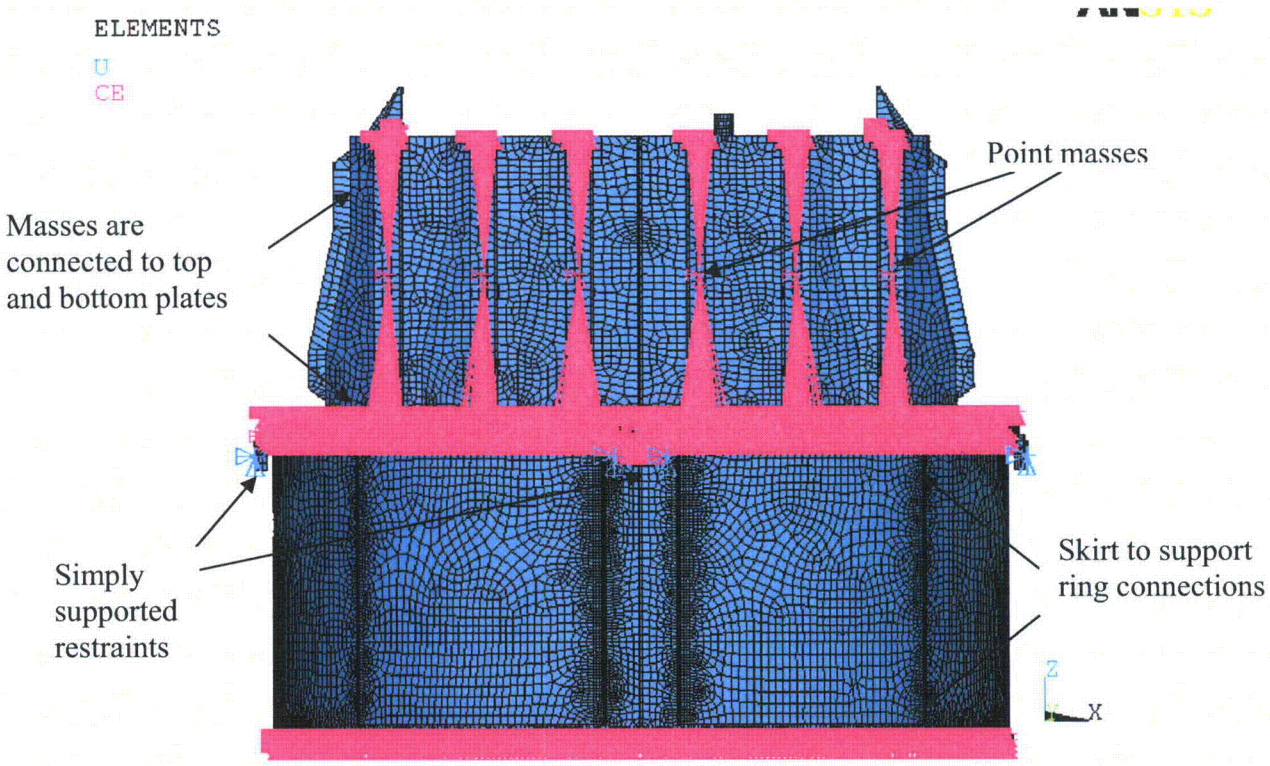

Figure 5. Point masses representing the vanes. The pink shading represents where constraint equations between nodes are applied.

Table 3. FE Model Summary.

Description	Quantity
Total Nodes[1]	133,622
Total Elements	119,408

1. Not including additional damper nodes and elements.

Table 4. Listing of Element Types.

Generic Element Type Name	Element Name	ANSYS Name
20-Node Quadratic Hexahedron	SOLID186	20-Node Hexahedral Structural Solid
10-Node Quadratic Tetrahedron	SOLID187	10-Node Tetrahedral Structural Solid
4-Node Elastic Shell	SHELL63	4-Node Elastic Shell
Mass Element	MASS21	Structural Mass
Pressure Surface Definition	SURF154	3D Structural Surface Effect
Beam element	BEAM188	3-D Finite Strain Beam
Damper element	COMBIN14	Spring-Damper

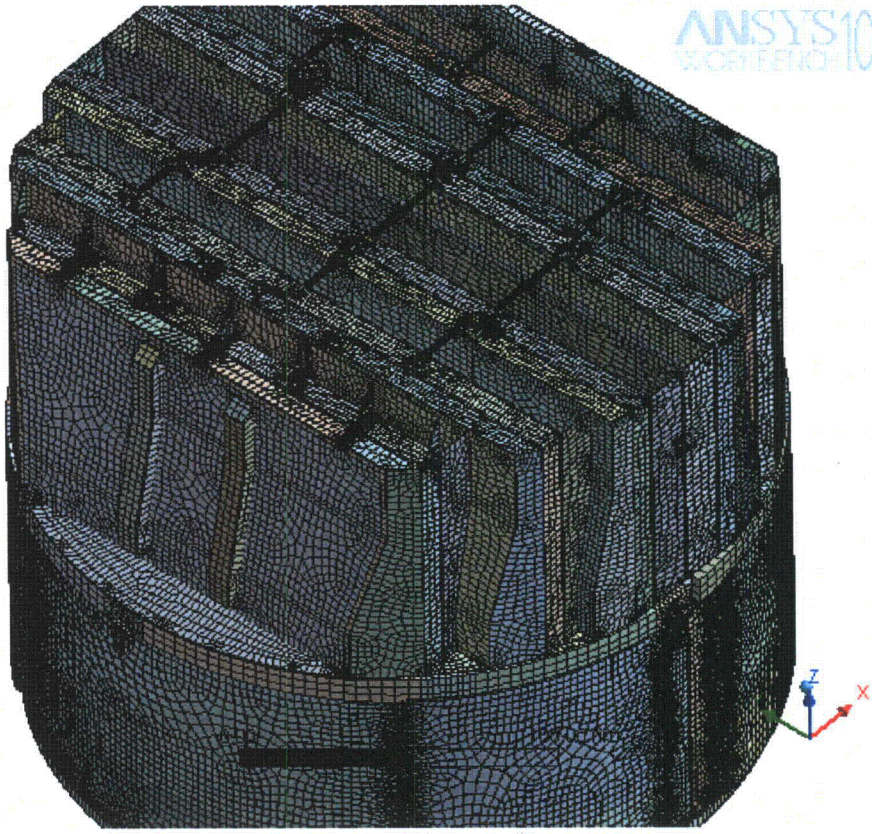

Figure 6a. Mesh overview.

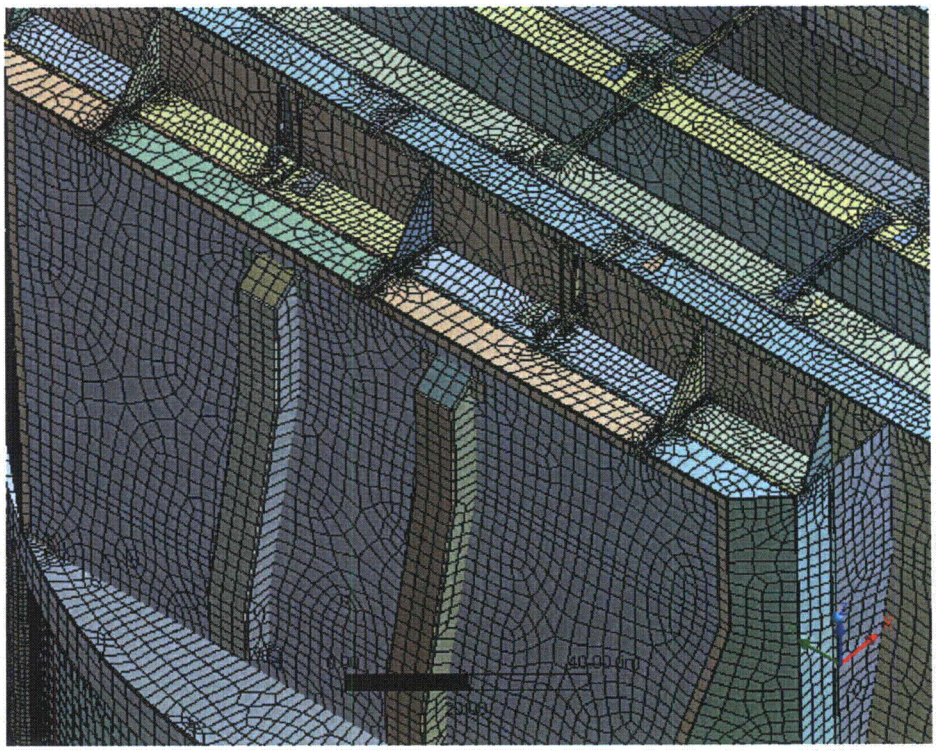

Figure 6b. Close-up of mesh showing hoods and hood assemblies.

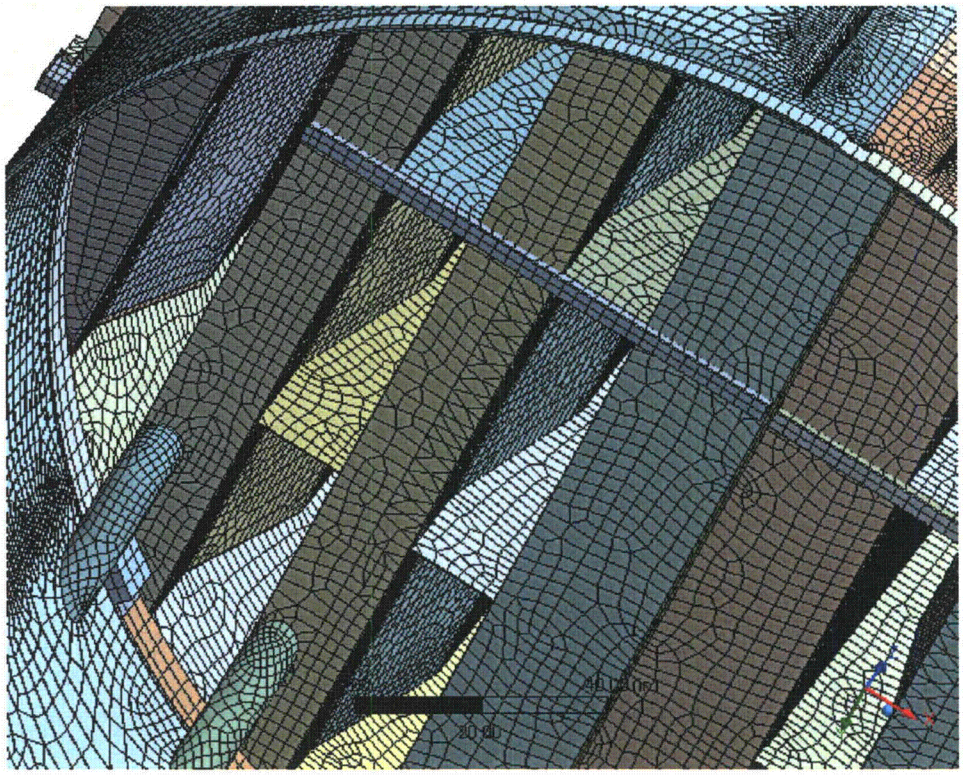

Figure 6c. Close-up of mesh showing drain pipes and hood supports; supporting beams and base plates.

Figure 6d. Close-up of mesh showing node-to-node connections between various plates.

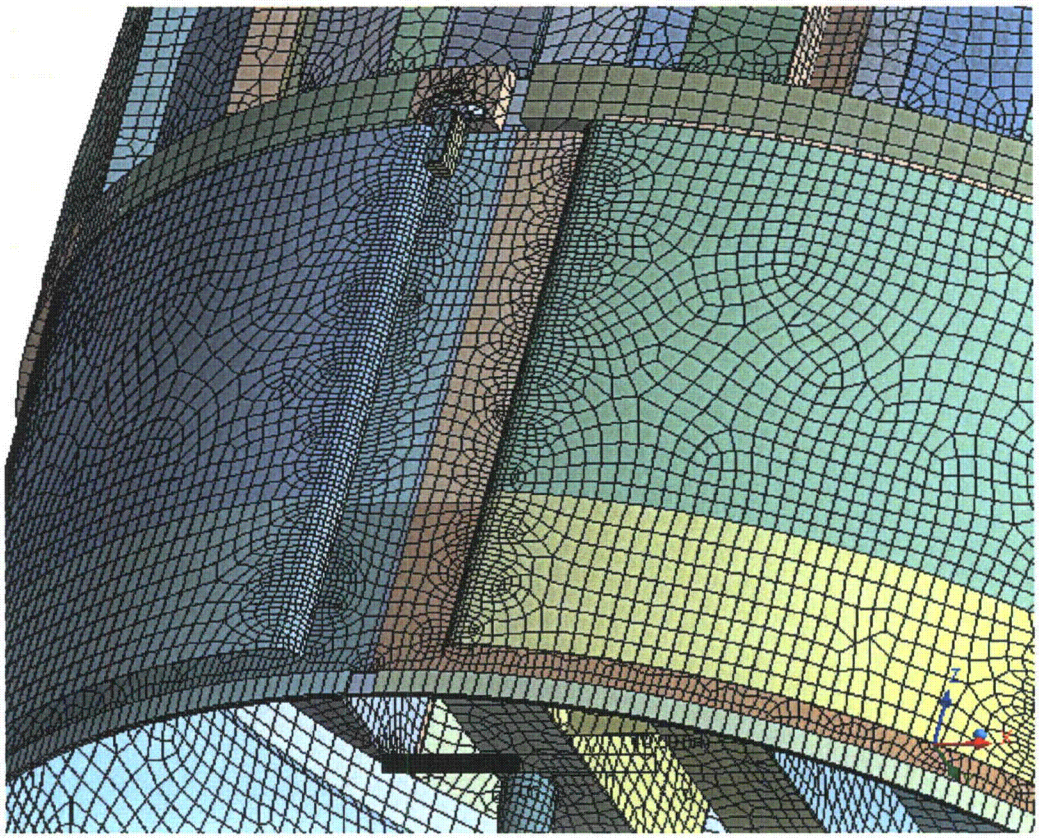

Figure 6e. Close-up of mesh showing node-to-node connections between the skirt and drain channels.

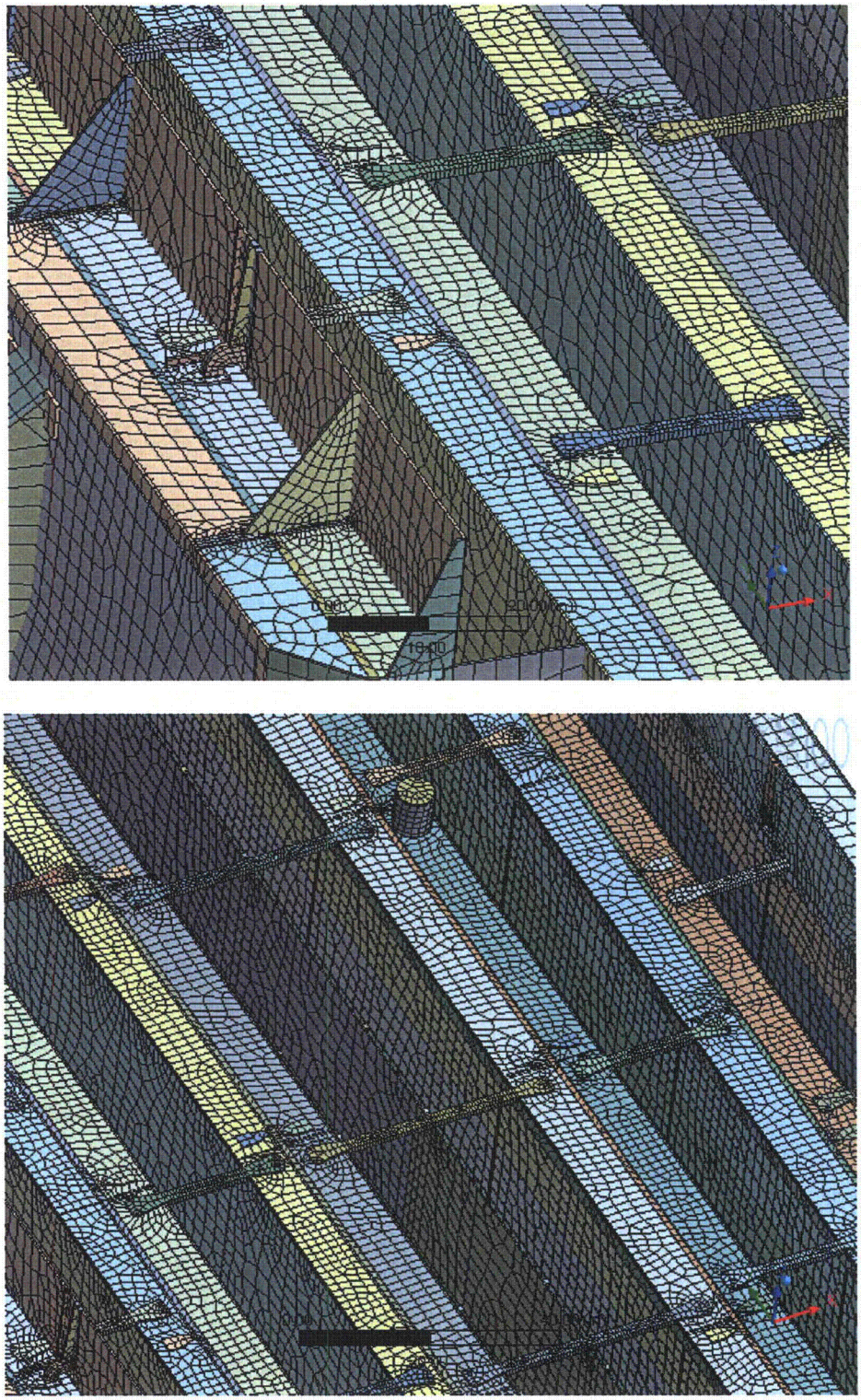

Figure 6f. Close-up view of tie bars connecting vane cover plates and adjacent to the steam dam.

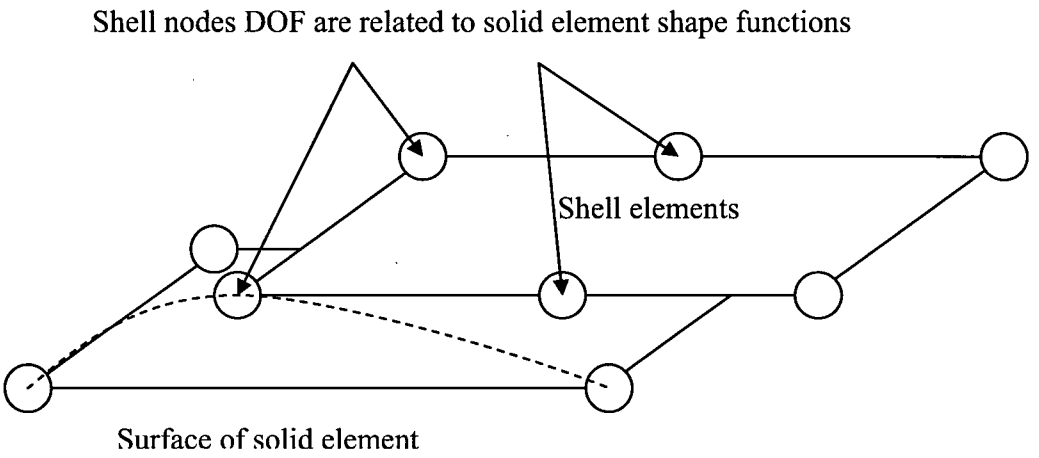

Figure 7a. Face-to-face shell to solid connection.

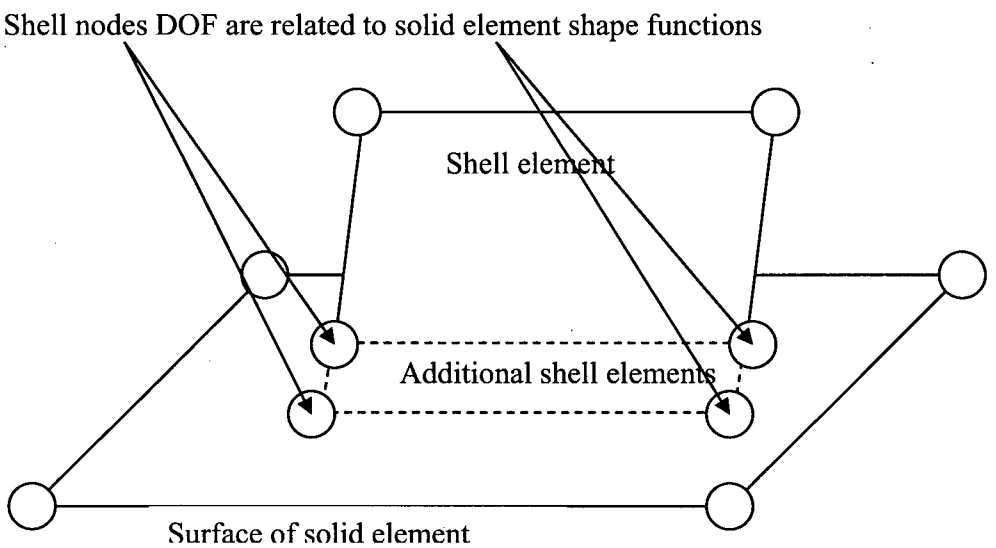

Figure 7b. Shell edge-to-solid face connection.

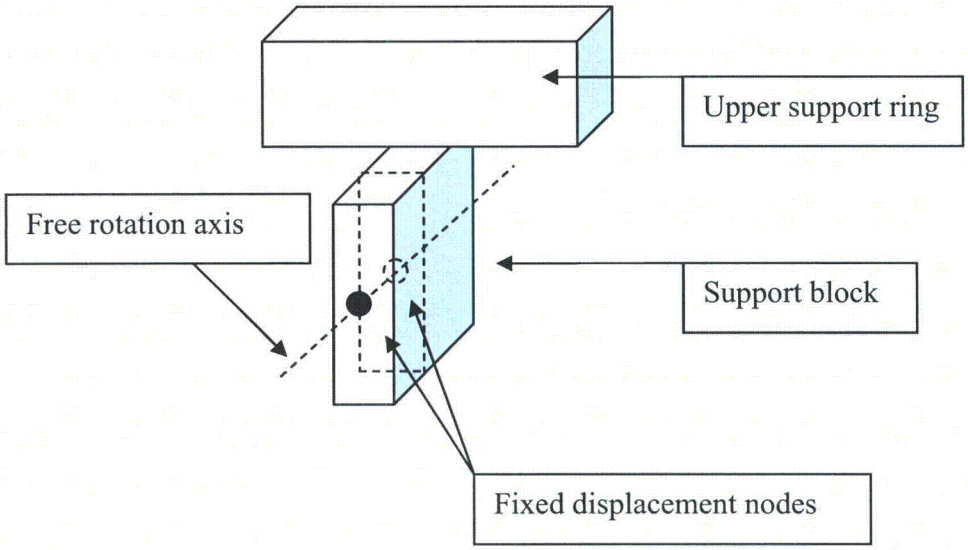

Figure 8. Boundary conditions. Inside node is half way between outer surface of support block and upper support ring.

3.10 Pressure Loading

The harmonic loads are produced by the pressures acting on the exposed surfaces of the steam dryer. At every frequency and for each MSL, the pressure distribution corresponding to a unit pressure at the MSL inlet is represented on a three-inch grid lattice grid (i.e., a mesh whose lines are aligned with the x-, y- and z-directions) that is superimposed over the steam dryer surface. This grid is compatible with the "TableLoads" format used by ANSYS to "paint" general pressure distributions upon structural surfaces. The pressures are obtained from the Helmholtz solver routine in the acoustic analysis [1].

In general, the lattice nodes do not lie on the surface, so that to obtain the pressure differences at the surface, it is necessary to interpolate the pressure differences stored at the lattice nodes. This is done using simple linear interpolation between the eight forming nodes of the lattice cell containing the surface point of interest. Inspection of the resulting pressures at selected nodes shows that these pressures vary in a well-behaved manner between the nodes with prescribed pressures. Graphical depictions of the resulting pressures and comparisons between the peak pressures in the original nodal histories and those in the final surface load distributions produced in ANSYS, all confirm that the load data are interpolated accurately and transferred correctly to ANSYS.

The harmonic pressure loads are only applied to surfaces above the water level, as indicated in Figure 9. In addition to the pressure load, the static loading induced by the weight of the steam dryer is analyzed separately. The resulting static and harmonic stresses are linearly combined to obtain total values which are then processed to calculate maximum and alternating stress intensities for assessment in Section 5.

[[

[3]]] This is useful since revisions in the loads model do not necessitate recalculation of the unit stresses.

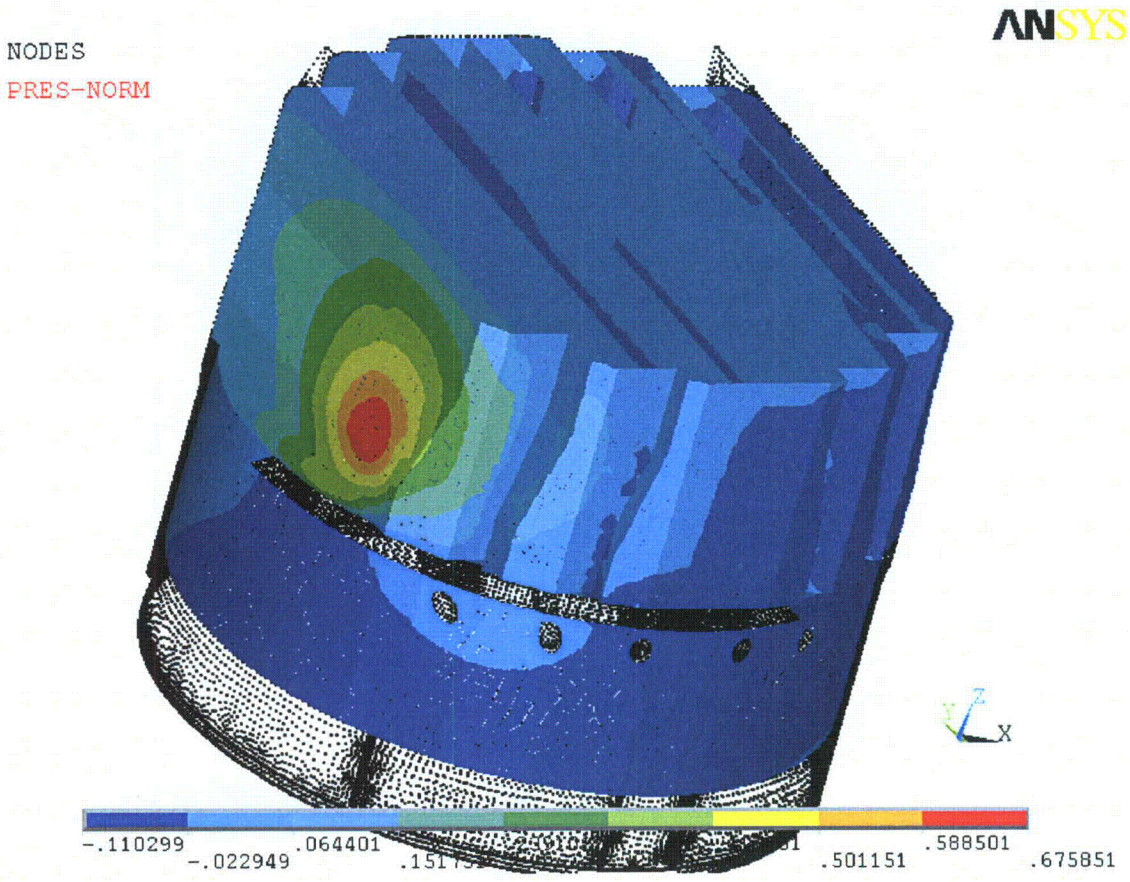

Figure 9a. Real part of unit pressure loading MSL C (in psid) on the steam dryer at 50.2 Hz. No loading is applied to the submerged surface.

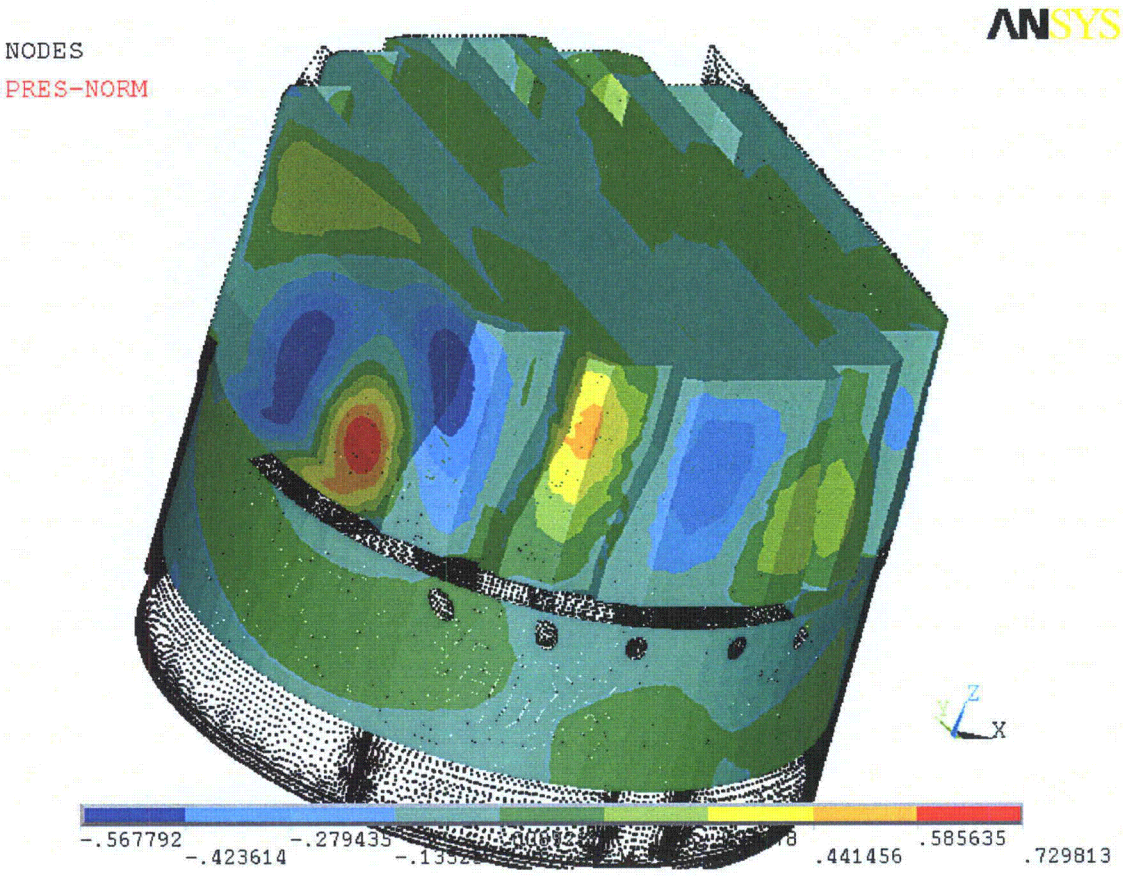

Figure 9b. Real part of unit pressure loading MSL C (in psid) on the steam dryer at 200.9 Hz. No loading is applied to the submerged surface.

4. Structural Analysis

The solution is decomposed into static and harmonic parts, where the static solution produces the stress field induced by the supported structure subjected to its own weight and the harmonic solution accounts for the harmonic stress field due to the unit pressure of given frequency in one of the main steam lines. All solutions are linearly combined, with amplitudes provided by signal measurements in each steam line, to obtain the final displacement and stress time histories. This decomposition facilitates the prescription of the added mass model accounting for hydrodynamic interaction and allows one to compare the stress contributions arising from static and harmonic loads separately. Proper evaluation of the maximum membrane and membrane+bending stresses requires that the static loads due to weight be accounted for. Hence both static and harmonic analyses are carried out.

4.1 Static Analysis

The results of the static analysis are shown in Figure 10. The locations with highest stress include the upper support ring areas near the support brackets with stress intensity 5,831 psi.

4.2 Harmonic Analysis

The harmonic pressure loads were applied to the structural model at all surface nodes described in Section 3.10. Typical stress intensity distributions over the structure are shown in Figure 11. Stresses were calculated for each frequency, and results from static and harmonic calculations were combined.

To evaluate maximum stresses, the stress harmonics including the static component are transformed into a time history using FFT, and the maximum and alternating stress intensities for the response, evaluated. According to ASME B&PV Code, Section III, Subsection NG-3216.2 the following procedure was established to calculate alternating stresses. For every node, the stress difference tensors, $\boldsymbol{\sigma}'_{nm} = \boldsymbol{\sigma}_n - \boldsymbol{\sigma}_m$, are considered for all possible pairs of the stresses $\boldsymbol{\sigma}_n$ and $\boldsymbol{\sigma}_m$ at different time levels, t_n and t_m. Note that all possible pairs require consideration, since there are no "obvious" extrema in the stress responses. However, in order to contain computational cost, extensive screening of the pairs takes place (see Section 2.3), so that pairs known to produce alternating stress intensities less than 1,500 psi are rejected. For each remaining stress difference tensor, the principal stresses S_1, S_2, S_3 are computed and the maximum absolute value among principal stress differences, $S_{nm} = \max\{|S_1 - S_2|, |S_1 - S_3|, |S_2 - S_3|\}$, obtained. The alternating stress at the node is then one-half the maximum value of S_{nm} taken over all combinations (n,m), i.e., $S_{alt} = \frac{1}{2}\max_{n,m}\{S_{nm}\}$. This alternating stress is compared against allowable values, depending on the node location with respect to welds.

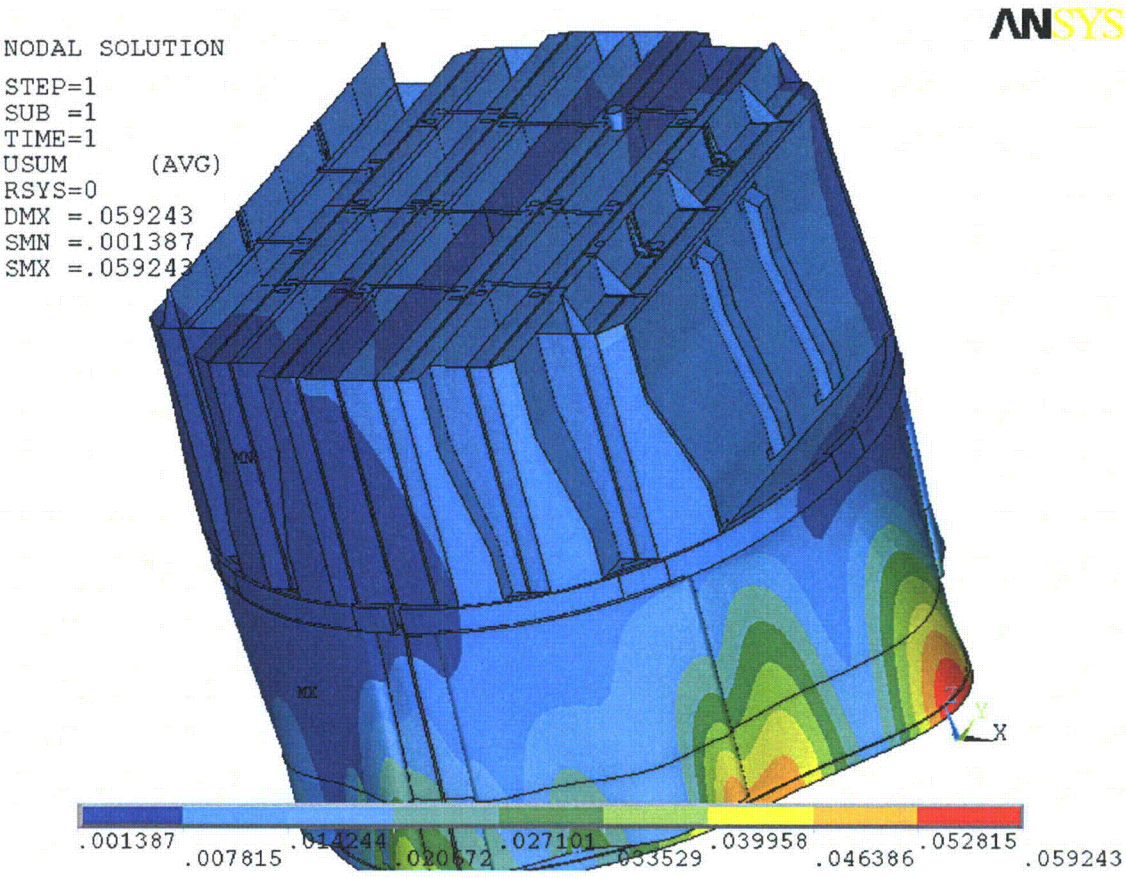

Figure 10a. Overview of static calculations showing displacements (in inches). Maximum displacement (DMX) is 0.06 inches. Note that displacements are amplified for visualization.

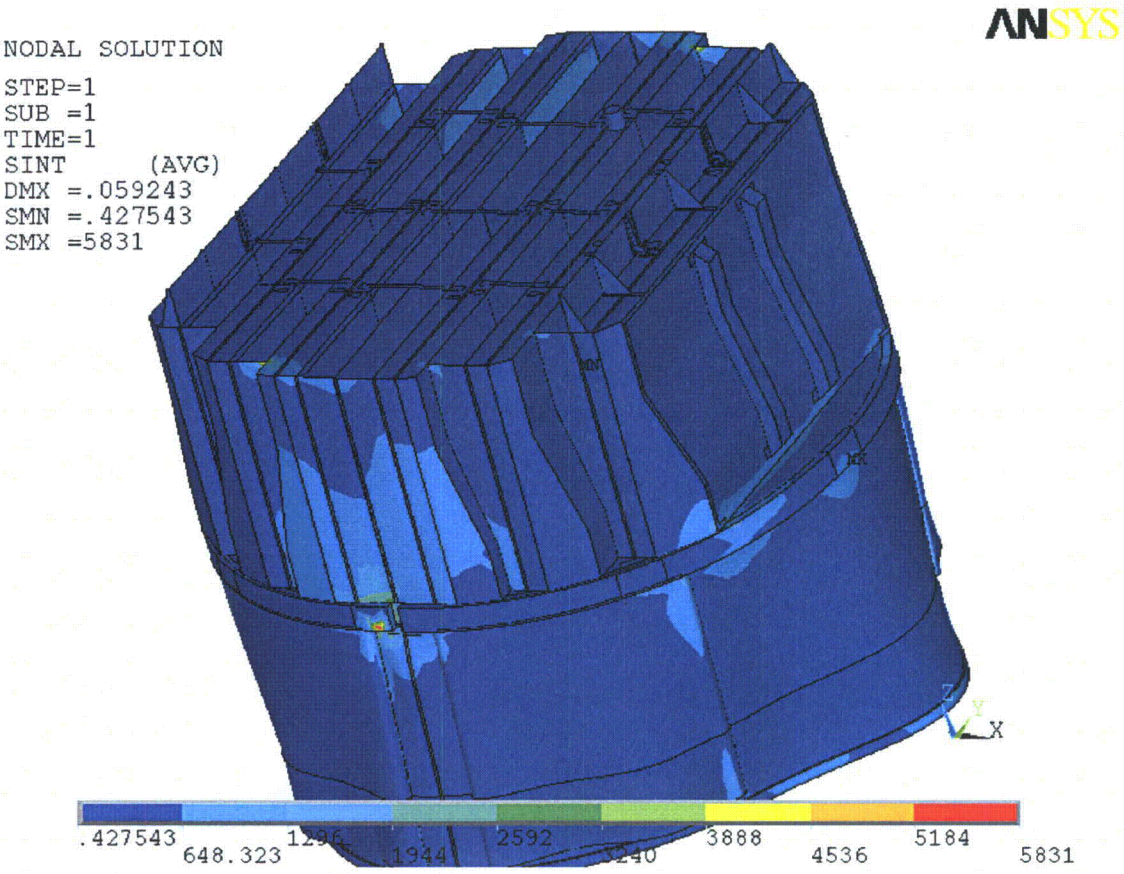

Figure 10b. Overview of static calculations showing stress intensities (in psi). Maximum stress intensity (SMX) is 5,831 psi. Note that displacements are amplified for visualization.

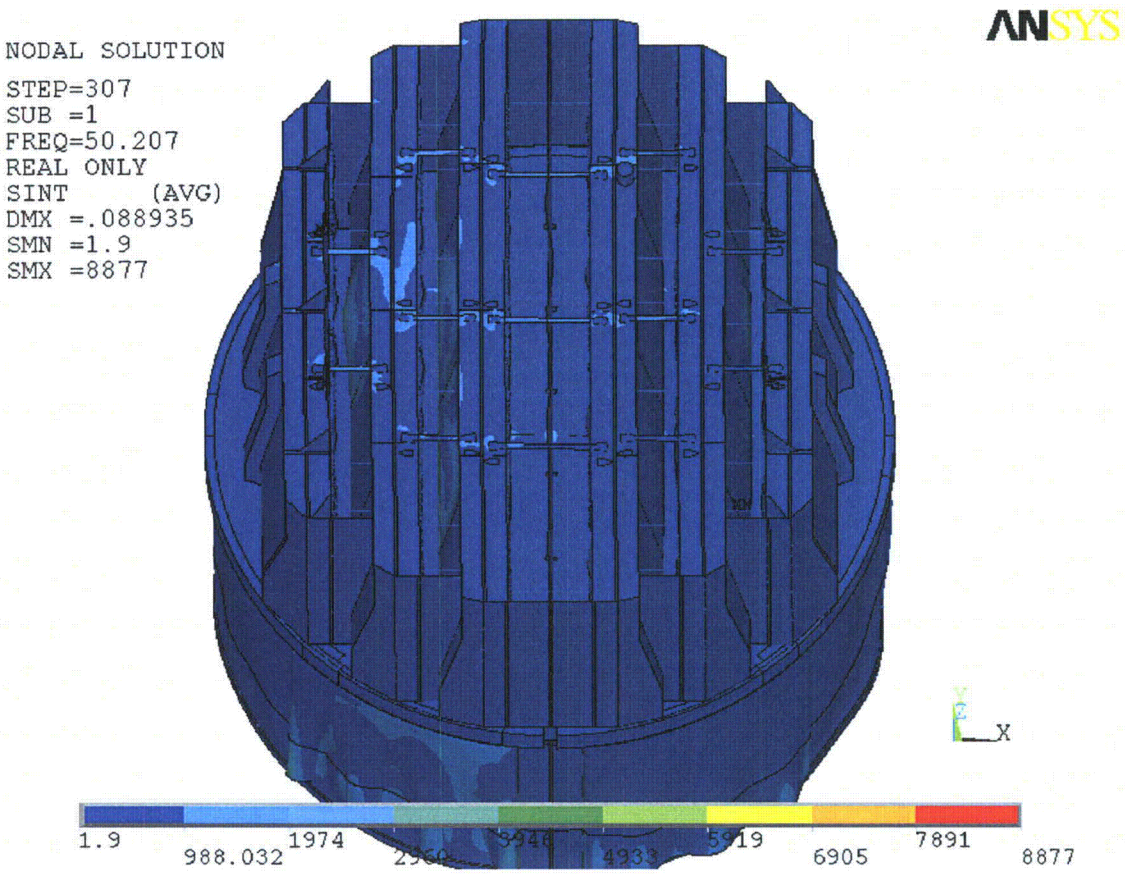

Figure 11a. Overview of harmonic calculations showing real part of stress intensities (in psi) along with displacements. Unit loading MSL C at 50.2 Hz.

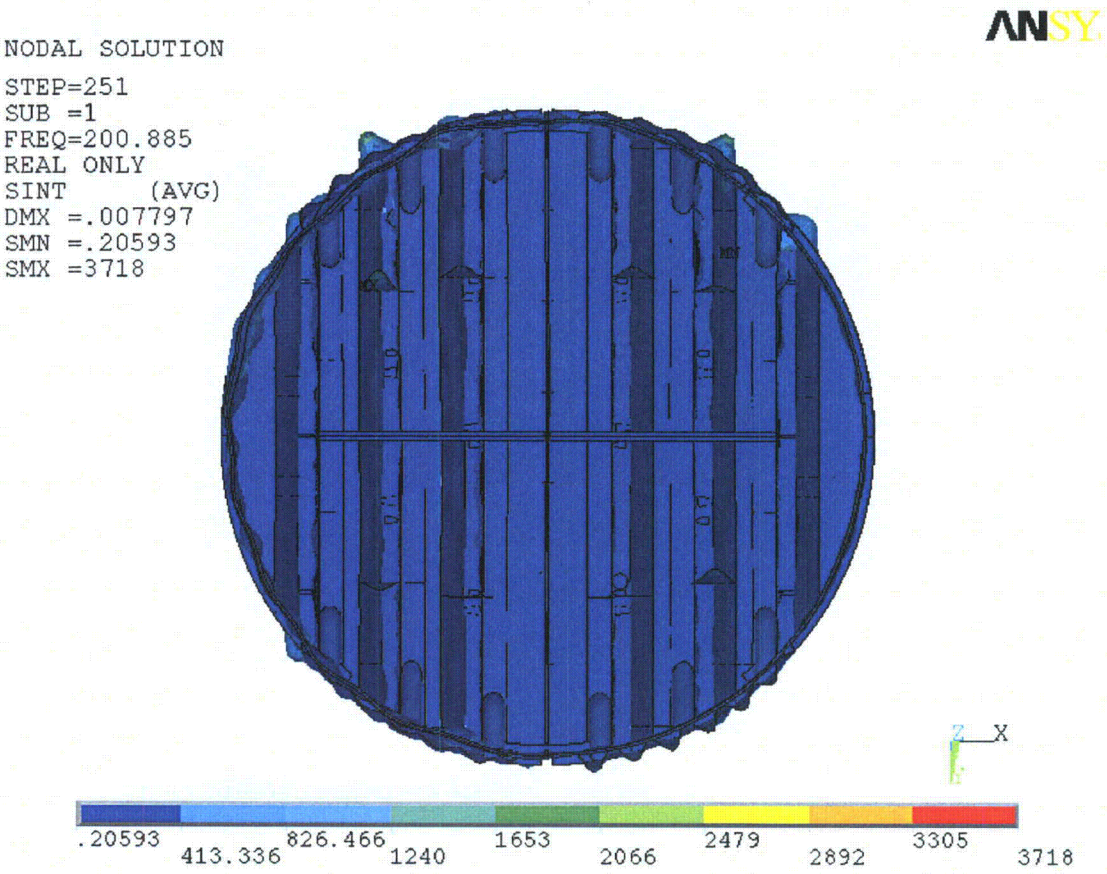

Figure 11b. Overview of harmonic calculations showing real part of stress intensities (in psi) along with displacements. Unit loading MSL C at 200.9 Hz.

4.3 Post-Processing

The static and transient stresses computed at every node with ANSYS were exported into files for subsequent post-processing. These files were then read into separate customized software to compute the maximum and alternating stresses at every node. The maximum stress was defined for each node as the largest stress intensity occurring during the time history. Alternating stresses were calculated according to the ASME standard described above. For shell elements the maximum stresses were calculated separately at the mid-plane, where only membrane stress is present, and at top/bottom of the shell, where bending stresses are also present.

For nodes that are shared between several structural components or lie on junctions, the maximum and alternating stress intensities are calculated as follows. First, the nodal stress tensor is computed separately for each individual component by averaging over all finite elements meeting at the node and belonging to the same structural component. The time histories of these stress tensors are then processed to deduce the maximum and alternating stress intensities for each structural component. Finally, for nodes shared across multiple components, the highest of the component-wise maximum and alternating stresses is recorded as the "nodal" stress. This approach prevents averaging of stresses across components and thus yields conservative estimates for nodal stresses at the weld locations where several components are joined together.

The maximum stresses are compared against allowable values which depend upon the stress type (membrane, membrane+bending, alternating – Pm, Pm+Pb, S_{alt}) and location (at a weld or away from welds). These allowables are specified in the following section. For solid elements the most conservative allowable for membrane stress, Pm, is used, although bending stresses are nearly always present also. The structure is then assessed in terms of stress ratios formed by dividing allowables by the computed stresses at every node. Stress ratios less than unity imply that the associated maximum and/or alternating stress intensities exceed the allowable levels. Post-processing tools calculate the stress ratios, identifying the nodes with low stress ratios and generating files formatted for input to the 3D graphics program, TecPlot, which provides more general and sophisticated plotting options than currently available in ANSYS.

4.4 Computation of Stress Ratios for Structural Assessment

The ASME B&PV Code, Section III, subsection NG provides different allowable stresses for different load combinations and plant conditions. The stress levels of interest in this analysis are for the normal operating condition, which is the Level A service condition. The load combination for this condition is:

Normal Operating Load Combination = Weight + Pressure + Thermal

The weight and fluctuating pressure contributions have been calculated in this analysis and are included in the stress results. The static pressure differences and thermal expansion stresses are small, since the entire steam dryer is suspended inside the reactor vessel and all surfaces are exposed to the same conditions. Seismic loads only occur in Level B and C cases, and are not considered in this analysis.

Allowable Stress Intensities

The ASME B&PV Code, Section III, subsection NG shows the following (Table 5) for the maximum allowable stress intensity (Sm) and alternating stress intensity (Sa) for the Level A service condition. The allowable stress intensity values for type 304 stainless steel at operating temperature 550°F are taken from Table I-1.2 and Fig. I-9.2.2 of Appendix I of Section III, in the ASME B&PV Code. The calculation for different stress categories is performed in accordance with Fig. NG-3221-1 of Division I, Section III, subsection NG.

Table 5. Maximum Allowable Stress Intensity and Alternating Stress Intensity for all areas other than welds. The notation Pm represents membrane stress; Pb represents stress due to bending; Q represents secondary stresses (from thermal effects and gross structural discontinuities, for example); and F represents additional stress increments (due to local structural discontinuities, for example).

Type	Notation	Service Limit	Allowable Value (ksi)
Maximum Stress Allowables:			
General Membrane	Pm	Sm	16.9
Membrane + Bending	Pm + Pb	1.5 Sm	25.35
Primary + Secondary	Pm + Pb + Q	3.0 Sm	50.7
Alternating Stress Allowable:			
Peak = Primary + Secondary + F	S_{alt}	Sa	13.6

When evaluating welds, either the calculated or allowable stress was adjusted, to account for stress concentration factor and weld quality. Specifically:

- For maximum allowable stress intensity, the allowable value is decreased by multiplying its value in Table 5 by 0.55.

- For alternating stress intensity, the calculated weld stress intensity is multiplied by a weld stress intensity (fatigue) factor of 1.8, before comparison to the Sa value given above.

The weld factors of 0.55 and 1.8 were selected based on the observable quality of the shop welds and liquid penetrant NDE or VT testing of all welds during fabrication (tack and intermittent welds, inner stiffeners and lower tie bars were subject to VT). These factors are consistent with fatigue strength reduction factors recommended by the Welding Research Council, [15], and stress concentration factors at welds, provided in [16] and [17]. In addition, critical welds are subject to periodical visual inspections in accordance with the requirements of GE SIL 644 SIL and BWR VIP-139 [18]. Therefore, for weld stress intensities, the allowable values are shown in Table 6.

These factors (0.55 and 1.8) also conservatively presume that the structure is joined using fillet welds unless specified otherwise. Since fillet welds correspond to larger stress concentration factors than other types of welds, this assumption is a conservative one. When the weld is known to be a full penetration weld a weld factor of 1.4 may be used. In the current analysis this is used for the weld joining the middle closure plate and inner hood.

Table 6. Weld Stress Intensities.

Type	Notation	Service Limit	Allowable Value (ksi)
Maximum Stress Allowables:			
General Membrane	Pm	0.55 Sm	9.30
Membrane + Bending	Pm + Pb	0.825 Sm	13.94
Primary + Secondary	Pm + Pb + Q	1.65 Sm	27.89
Alternating Stress Allowables:			
Peak = Primary + Secondary + F	S_{alt}	Sa	13.6

Comparison of Calculated and Allowable Stress Intensities

The classification of stresses into general membrane or membrane + bending types was made according to the exact location, where the stress intensity was calculated; namely, general membrane, Pm, for middle surface of shell element, and membrane + bending, Pm + Pb, for other locations. For solid elements the most conservative, general membrane, Pm, allowable is used.

The structural assessment is carried out by computing stress ratios between the computed maximum and alternating stress intensities, and the allowable levels. Locations where any of the stresses exceed allowable levels will have stress ratios less than unity. Since computation of stress ratios and related quantities within ANSYS is time-consuming and awkward, a separate FORTRAN code was developed to compute the necessary maximum and alternating stress intensities, Pm, Pm+Pb, and S_{alt}, and then compare it to allowables. Specifically, the following quantities were computed at every node:

1. The maximum membrane stress intensity, Pm (evaluated at the mid-thickness location for shells),
2. The maximum membrane+bending stress intensity, Pm+Pb, (taken as the largest of the maximum stress intensity values at the bottom, top, and mid thickness locations, for shells),
3. The alternating stress, S_{alt}, (the maximum value over the three thickness locations is taken).
4. The stress ratio due to a maximum stress intensity assuming the node lies at a non-weld location (note that this is the minimum ratio obtained considering both membrane stresses and membrane+bending stresses):
   SR-P(nw) = min{ Sm/Pm, 1.5 * Sm/(Pm+Pb) }.
5. The alternating stress ratio assuming the node lies at a non-weld location,
   SR-a(nw) = Sa / (1.1 * S_{alt}),
6. The same as 4, but assuming the node lies on a weld,
   SR-P(w)=SR-P(nw) * 0.55
7. The same as 5, but assuming the node lies on a weld,
   SR-a(w)=SR-a(nw) / 1.8. (for the full penetration weld connecting the middle closure plate and inner hood a weld factor of 1.4 instead of 1.8 is used so that SR-a(w) = SR-a(nw) / 1.4)

Also for undersized welds undersize weld factors are applied to the stresses when computing stress ratios. In the present analysis undersize weld factors are used in two locations known to be undersized: the horizontal weld connecting the T-bar and base plates (the undersize weld factor, f_{usw}=2) and the vertical weld connecting the steam dam to the end gussets (f_{usw}=1.5 – note that these gusset welds will be reinforced prior to EPU operation to restore an appropriately sized weld so that no undersize weld factor will be needed). Note that in steps 4 and 6, the minimum of the stress ratios based on Pm and Pm+Pb, is taken. The allowables listed in Table 5, Sm=16,900 psi and Sa=13,600 psi. The factors, 0.55 and 1.8 (or 1.4 for the cited full penetration groove weld), are the weld factors discussed above. The factor of 1.1 accounts for the differences in Young's moduli for the steel used in the steam dryer and the values assumed in alternating stress allowable. According to NG-3222.4 in subsection NG of Section III of the ASME Code, the effect of elastic modulus upon alternating stresses is taken into account by multiplying alternating stress S_{alt} at all locations by the ratio, E/E_{model}=1.1, where:

$E = 28.3\ 10^6$ psi, as shown on Fig. I-9.2.2. ASME BP&V Code
$E_{model} = 25.55\ 10^6$ psi (Table 1)

The appropriate maximum and alternating stress ratios, SR-P and SR-a, are thus determined and a final listing of nodes having the smallest stress ratios is generated. The nodes with stress ratios lower than 4 are plotted in TecPlot (a 3D graphics plotting program widely used in engineering communities [19]). These nodes are tabulated and depicted in the following Results Section.

4.5 Finite Element Sub-modeling

In order to maintain computational costs at a feasible level, the steam dryer model is predominantly comprised of shell elements. These elements are well suited for structures such as the steam dryer consisting of shell-like components and tend to produce conservative estimates of the stresses. In some cases however, such as welded junctions involving multiple components, shell element models can overestimate the nominal stress intensities in the vicinity of the junctions. In such cases a more refined analysis using solid elements to capture the complete 3D stress distribution, is warranted. Therefore, to efficiently analyze complex structures such as steam dryers, a standard engineering practice is to first analyze the structure using a shell-based model. If any locations with high stresses are identified these regions are examined in greater detail using 3D solid elements to obtain a more definitive stress prediction.

In the BFN1 steam dryer, four locations shown in Figure 12 were identified as requiring a more refined stress analysis: (i) the bottom of the skirt/drain channel junction; (ii) the intersection between the bottom of the inner hood, hood support (stiffener) and base plate; (iii) the weld connecting the mid-height tie bars to the perforated plates and (iv) the inner hood/hood support weld. The first location is characterized by a previously thickened continuous weld that wraps around the bottom of the drain channel and up along the interior of the channel. The second location involves the junction between three elements and experienced an alternating stress ratio of SR-a=2.62 in [8]. Although this stress ratio is comparatively high, it is nevertheless of concern because it is difficult to access. The third location experiences stress ratios slightly below the target level (SR-a=1.96 at 110% OLTP) when the biases and uncertainties are revised over the new frequency intervals. The fourth location also is difficult to

access and experienced a stress ratio of SR-a=2.11 at 110% OLTP when the revised biases and uncertainties are used and low power noise is left in.

These locations were examined using the 3D solid element sub-modeling procedures described in [20] and Appendix A of [21], and validated against both high resolution solid models of the full structure and sub-structuring results in [22] and [23]. Results for the first two locations were reported in [20]. The third and fourth locations were similarly analyzed using the approach in Appendix A of [21]. In each of the last two cases a 6"×6"×6" sub-model is extracted from the global model. The sub-model is first represented using shell elements and a combination of perimeter forces on the intersection edges and a distributed body force applied to match the component stresses in the vicinity of the high stress location. The stress intensity at the high stress location is calculated which for sub-models 3 and 4 are 3994 psi and 3165 psi respectively. Next, a highly detailed solid element representation of the sub-model including the welds is generated. The same forces and body force distribution are applied to this solid element sub-model and the stresses calculated. Linearized stresses are extracted from several paths in the weld [20-23] and the highest such stress identified. For sub-models 3 and 4 these are 2003 psi and 2364 psi. The stress reduction factors (SRFs) are obtained as the ratio between the shell- and solid-element sub-model stresses.

Based on these models, the nominal stress intensities computed by the 3D solid element model are lower than those obtained with the shell-based FEA used to analyze the complete steam dryer by factors of (see Table 7): (i) 0.58 for the bottom inch of the skirt/drain channel weld (a total of sixteen nodes) and (ii) 0.79 for the inner hood/hood support/base plate junction (a total of four nodes); (iii) 0.5 for the tie bar/perforated plate connections and (iv) 0.77 for the inner hood/hood support weld. The variation of stress reduction factor among these locations is strictly dependent on the individual geometry and general loading characteristics. The discontinuity stresses computed in a shell model at a weld joint between two orthogonal members are often quite conservative because the shell element depiction does not provide any credit for the stress distribution associated with the specific weld geometry. The stress intensities predicted by the shell element-based analysis at these locations are therefore first multiplied by these factors to obtain more accurate estimates of the nominal stresses. These are then multiplied by the 1.8 weld factor before comparing against allowable values to obtain the alternating stress ratios.

Table 7. Summary of stress reduction factors obtained using sub-model analysis.

	Location	Stress Reduction Factor
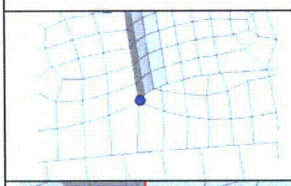	1. Last 1" at bottom of drain channel/skirt weld	0.58
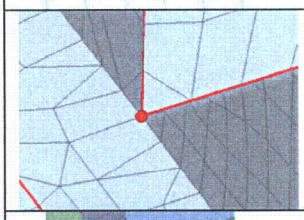	2. Inner hood/hood support/middle base plate	0.79
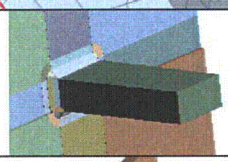	3. Mid-height tie-bar/perforated plate	0.50
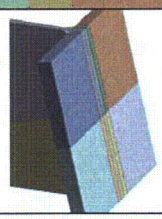	4. Inner hood/hood support	0.77

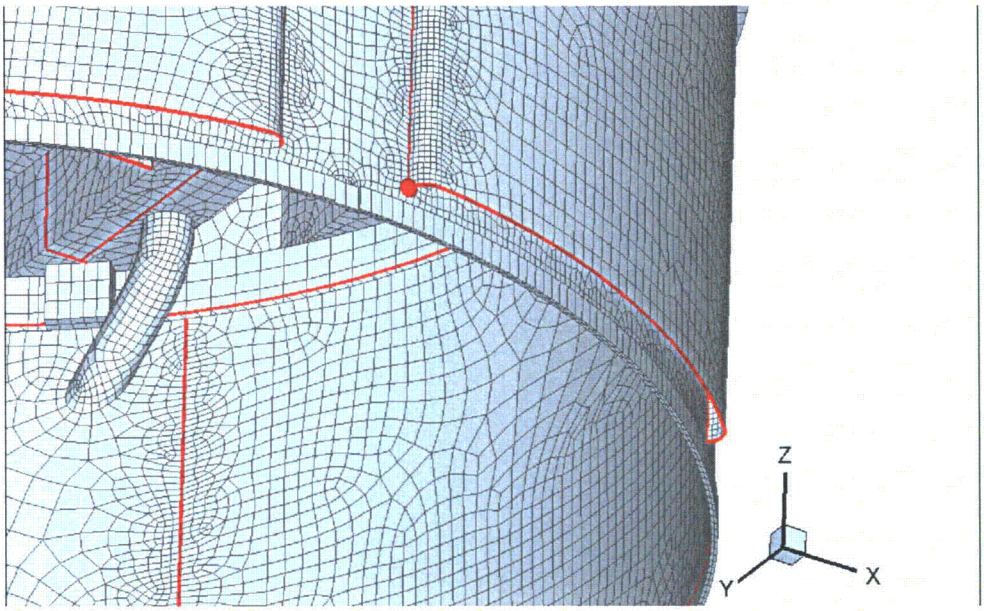

Figure 12a. Location of node on drain channel/skirt weld analyzed with sub-model in [20].

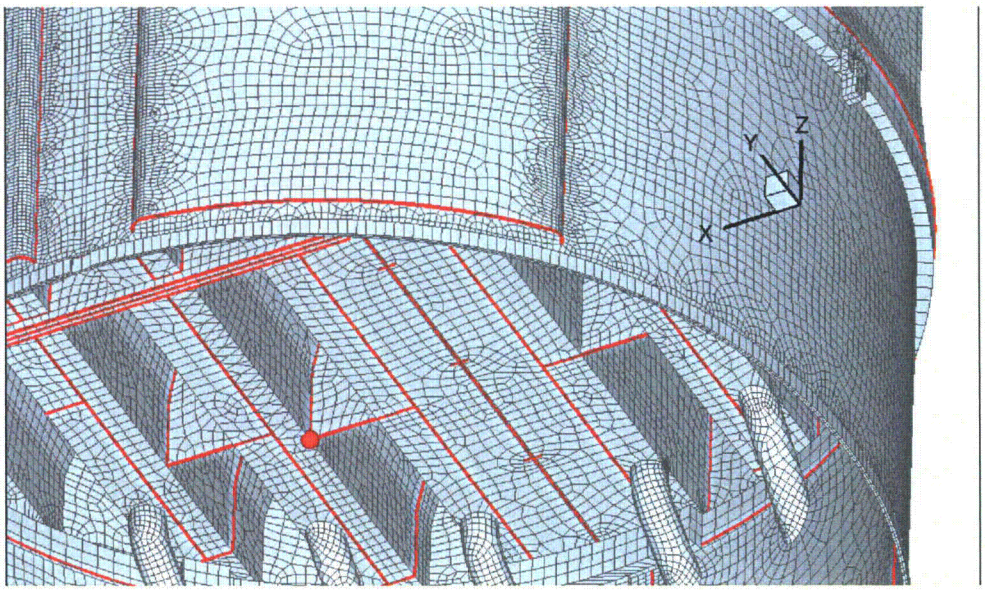

Figure 12b. Location of node on inner hood/hood support/middle base plate weld analyzed with sub-model in [20].

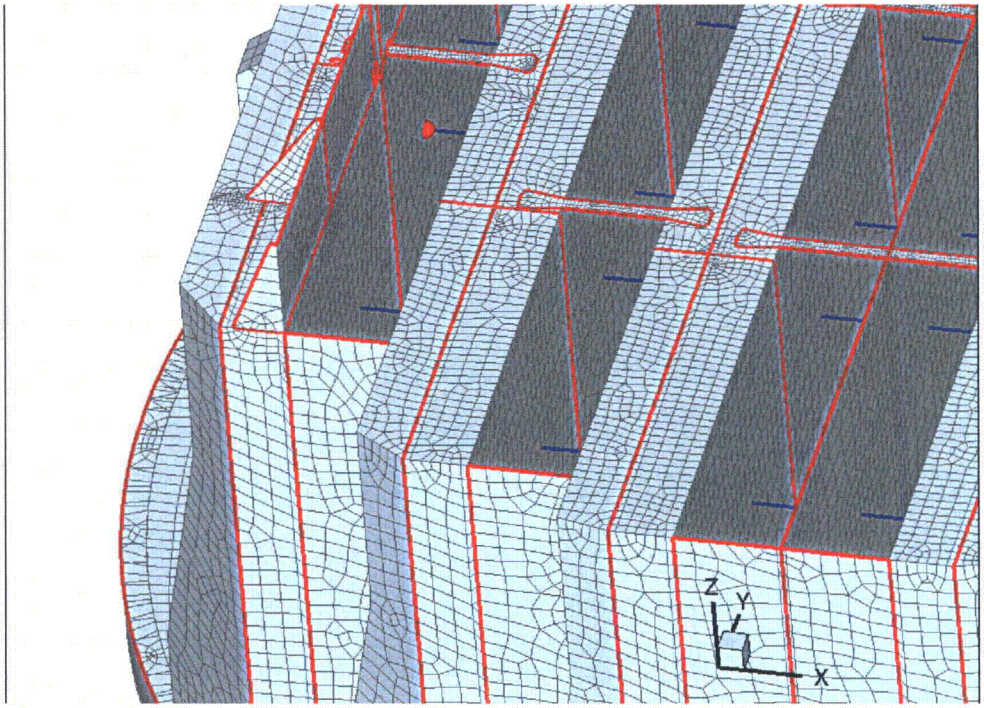

Figure 12c. Location of node on tie bar/perforated plate weld analyzed with sub-model analysis procedure in Appendix A of [21].

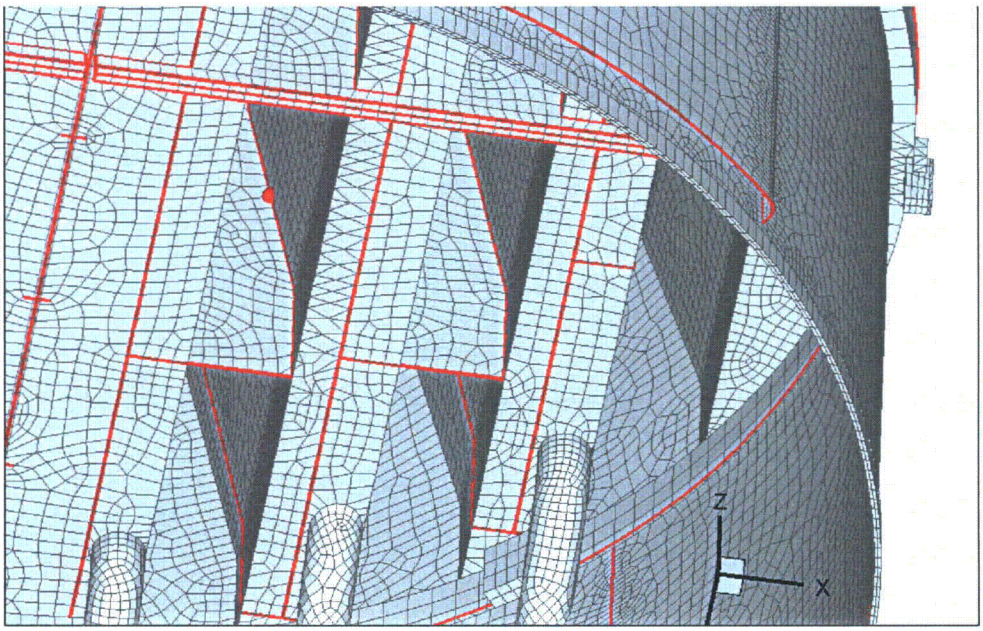

Figure 12d. Location of node on inner hood/hood support weld analyzed with sub-model analysis procedure in Appendix A of [21].